Growth of composition-modulated Ag/Co wires on Pt(997)

P. Gambardella, M. Blanc, K. Kuhnke, and K. Kern
Institut de Physique Expérimentale, Ecole Polytechnique Fédérale de Lausanne, CH-1015 Lausanne, Switzerland and Max-Planck-Institut für Festkörperforschung, Heisenbergstrasse 1, D-70569 Stuttgart, Germany

F. Picaud, C. Ramseyer, and C. Girardet
Laboratoire de Physique Moléculaire, UMR CNRS 6624, Faculté des Sciences, La Bouloie, Université de Franche-Comté, 25030 Besançon Cedex, France

C. Barreteau, D. Spanjaard, and M. C. Desjonquères
Laboratoire de Physique des Solides, Université de Paris Sud, 91405 Orsay, France and SRSIM-CEA, 91191 Gif sur Yvette, France

(Received 26 July 2000; revised manuscript received 15 February 2001; published 28 June 2001)

Sequential deposition of Ag and Co on a Pt(111) stepped surface has been investigated as a means to obtain composition-modulated atomic wires. Thermal energy He atom scattering in grazing incidence conditions allows us to control and characterize the growth of Ag/Co wires on Pt(997) as a function of the substrate coverage and temperature. When Co is deposited first, Ag and Co atoms arrange themselves into regular stripes parallel to the Pt steps. A disordered phase is obtained when Ag is deposited first. We have carried out calculations based on semiempirical potentials to study the equilibrium configuration of a Ag/Co mixture on Pt(997). The experimental observations agree with ground-state calculations of the atomic structure, indicating that the first pure Co row in contact with the Pt step edge is very stable while the second row is occupied by Ag atoms. Free-energy minimization using a mean-field Ising approach at finite temperature of equimolar binary mixtures leads to very consistent results for the Ag/Co system, namely the preferential sequence with nearly pure Co and Ag wires in the first and second rows at the step. Predictive extensions to Co/Cu and Ag/Cu systems are discussed within the same approach. A preferential ordering with Co (Cu) occupying the first row and Cu (Ag) the second row is clearly obtained from the calculations, although the Ag/Cu system can also be frozen in reverse order.

DOI: 10.1103/PhysRevB.64.045404 PACS number(s): 68.65.−k, 34.20.−b, 61.66.Dk, 68.35.Md

I. INTRODUCTION

Epitaxy of multicomponent metal films is a widely studied subject because of its relevance for technological applications in the areas of catalysis, microelectronics, and material science.[1,2] Understanding the interplay between heteronuclear metal-metal bonds, surface geometric structure, and overlayer morphology is a prerequisite for elaborating mixed-metal compounds with tailored structural and electronic properties. The morphological and chemical characteristics of the interface between two metals can critically influence the physical behavior of low-dimensional systems. Interfaces between magnetic and nonmagnetic materials are of special interest because of their influence on the magnetic anisotropy of thin films[3–6] and on the electronic transport properties of multilayered devices.[7–10] Ag/Co multilayers, in particular, exhibit giant magnetoresistance properties[11] and bulk immiscibility of the two constituents. As a consequence, they have been the object of numerous studies that looked at the connection between structure and transport properties.[9,12,13] Quite naturally, most of the attention to date has been directed towards two-dimensional (2D) layered films, since many devices used for microelectronics or magnetorecording applications are based on multilayer structures. However, technological progress will likely require devising and characterizing more complex structures in less than two dimensions.

In this paper, we test and analyze a method to grow ordered arrays of parallel wires of alternate Ag/Co composition. Sequential evaporation of two metals on a vicinal surface can be used to fabricate lateral superlattices with a tunable periodic structure, as has been demonstrated for semiconductor systems.[14] To obtain sharp interfaces between the different elements, this technique requires detailed knowledge of the lateral adatom interaction as well as of the adsorbate-substrate potential. Here we investigate experimentally and theoretically the formation and stability of one-dimensional (1D) Ag/Co wires obtained by step decoration of the vicinal Pt(997) surface. Thermal energy atom scattering (TEAS) can be successfully employed to monitor *in situ* and in real time the growth of 1D aggregates on stepped surfaces,[15–18] as well as 2D layer-by-layer growth.[19,20] In previous studies,[15,16,21] we have shown that the deposition of Ag (Co) on Pt(997) in the appropriate temperature range results in the row-by-row growth of 1D atomic wires at the bottom of the Pt step edges. By subsequent deposition of Co (Ag), we obtain the formation of a thicker wire of mixed composition whose structure depends on the order of evaporation and on the surface temperature.

The experimental observations are compared to ground-state calculations of the atomic structure and to thermodynamic results issued from a model of row formation that support the experimental data. In particular, we show how the compositional and morphological characteristics of the

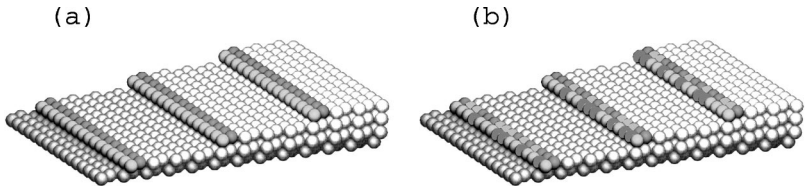

FIG. 1. (a) Pictorial view of the Pt(997) surface. The darker atoms at the step edges represent Co and Ag atoms forming ordered 1D chains. (b) Ag/Co alloy wire at the step edge.

Ag/Co structures depend on the surface geometry and on the bonding between the different species. In the bulk, both Ag and Co and Ag and Pt are immiscible, while Co and Pt alloy in a wide range of temperature and composition. Although surface-confined alloys exist for Ag/Pt (Ref. 22) and Ag/Co,[23,24] we will see that the stronger tendency to alloying of Co and Pt affects the composition of the Ag/Co wires. Semiempirical potentials are used to determine stable configurations at 0 K for the single metal adsorbate and then for an equimolar mixture of two adsorbates. Then equilibrium thermodynamic principles are used, within the mean-field Ising approximation, to discuss the row formation process in an equimolar binary alloy at finite temperature.

The paper is organized as follows. Section II is devoted to the presentation of the experimental results on Ag/Co epitaxy on Pt(997). We start by presenting the results for pure Ag and Co wires (Sec. II A) and we describe successively the Ag/Co wires (Sec. II B). In Sec. III, the results of the ground-state calculations of the wire structure using semiempirical interaction potentials are given for single and mixed metal adspecies. The thermodynamic model is presented and applied to the Ag/Co, Co/Cu, and Ag/Cu binary mixtures in Sec. IV.

II. EXPERIMENT

The TEAS measurements have been carried out in a high-resolution He scattering spectrometer[25,26] at a He wavelength $\lambda_{He}=0.92$ Å. The apparatus allows independent variation of the incidence angle θ_i and reflection angle θ_f for $60° \leqslant \theta_i + \theta_f \leqslant 180°$. The Pt sample is mounted on a cryostat that allows the temperature to be varied between 40 K and 1100 K. The Pt(997) surface consists of close-packed (111) terraces with a hexagonal lattice parameter of 2.77 Å separated by monatomic steps with {111} microfacets, 2.27 Å in height (Fig. 1). The average terrace width is 20.1 Å (or eight atomic rows), with a distribution that is remarkably narrow (standard deviation ~ 3 Å) due to repulsive interaction between the steps.[27] The surface is prepared by repeated cycles of 800-eV Ar^+ sputtering and annealing to 850 K, followed by a brief oxygen exposure at a pressure of 1×10^{-7} and by flash annealing at $T>1000$ K to remove possible carbon contaminants. Cleanliness is checked by Auger and He reflectivity measurements; the base pressure in the sample chamber is 1×10^{-10} mbar. Ag and Co are evaporated with two electron-beam evaporators with typical deposition rates of a few 10^{-3} ML s^{-1} (ML denotes monolayer).

A. Growth of pure Ag and Co wires

The decoration of Pt steps by Ag or Co adatoms is characterized by monitoring the intensity of the He beam reflected by the surface during evaporation. In general, He scattering on a vicinal surface gives rise to a diffraction pattern whose maxima are located at the Bragg positions corresponding to the periodic arrangement of terraces. As in an optical blazed reflection grating, the most intense diffraction orders are tilted away from the specular direction. Here we take advantage of this fact to enhance the contribution from the step to the reflected He intensity over the one from the terrace. In the specular direction the intensity coming from the flat terrace regions is very low; on the other hand, due to the bending of the repulsive He-surface potential at step edges, the intensity of the reflected beam at grazing exit angles (large θ_f) originates mainly from the interaction of He atoms with atoms near the step.[18,28,29] Specular scattering conditions ($\theta_i=\theta_f$) for large θ_f values are therefore suited for the investigation of processes that take place at the substrate step edges. Step sensitivity is further enhanced by the large θ_i values, which cause the shadowing of the terrace regions close to the steps.

For given scattering parameters θ_i, θ_f, and λ_{He}, the variations of the He reflected intensity depend only on the surface topmost layer structure, the intensity being a decreasing function of the density of diffuse scatterers on the surface.[19,20,30] Ordered structures that present a minimum of kinks and defects therefore correspond to intensity maxima. In grazing incidence conditions, the He reflectivity changes between complete and incomplete adatom rows at step edges. In Fig. 2, we report the intensity of the He beam reflected at grazing angles ($\theta_i=\theta_f=83°$) from the surface during deposition of Ag [Fig. 2(a)] and Co [Fig. 2(b)]. The coverage scale has been calibrated by repeating the same measurements at $\theta_i=60°$, $\theta_f=47°$: the sensitivity to terrace ordering in this case allowed us to determine precisely the monolayer position, as reported in Refs. 15 and 16. The reflected intensity has been normalized to its initial value prior to deposition. The decrease in intensity during the first evaporation stage can be qualitatively explained as follows. As Ag or Co adatoms arrive on the surface, they migrate to the step edges where the increase in coordination results in stronger bonding (see Sec. III B). Since the terrace width is very short compared to the mean free path of the adatoms in the 150 K–250 K temperature range adopted in this work, there is no nucleation on terraces. Adatoms arriving at the step sites can move along the Pt edges until they nucleate in stable 1D clusters.[15,16] Both single adatoms and the 1D cluster edges at steps constitute diffuse scatterers for the He beam. The reflected intensity decreases until the defect density at the steps reaches a maximum and then starts recovering as the vacancies in the growing row begin to fill. The first and most intense peak in the two curves therefore corresponds to the nucleation of a continuous monatomic row of adatoms along the Pt lower step edges. The coverage corre-

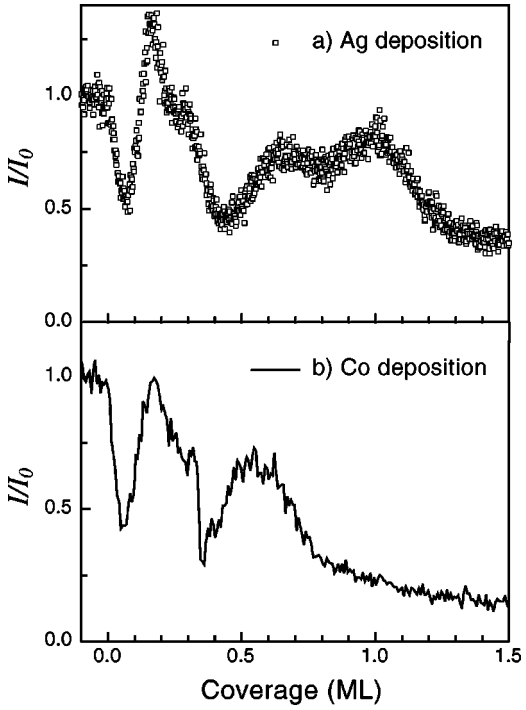

FIG. 2. Normalized intensity of the specularly reflected He beam during Ag (a) and Co (b) deposition at $T=250$ K in grazing incidence conditions, $\theta_i=\theta_f=83°$. The maximum at ~ 0.17 ML corresponds to the completion of the first monatomic row along the Pt step edges; see text for further explanations.

sponding to this peak is about 0.17 ML, slightly larger than the nominal coverage of 0.13 ML of a pseudomorphic row decorating the steps of a Pt(997) surface. This coverage shift is a temperature effect: as shown in Refs. 15,16, and 21, at $T\leqslant 250$ K, edge diffusion processes are not completely effective in rearranging all adatoms along the Pt edges. A fraction of migrating adatoms that stick to Ag or Co atoms already decorating the Pt steps cannot reach the remaining undecorated Pt sites, and when the first row has been completed, nucleation of the second row has already begun. In this work, the temperature has been nonetheless kept below 250 K in order to minimize surface intermixing between Co and Pt.[16]

Observation of row-by-row growth beyond the first one is hindered by the loss of growth coherence between different terraces. Since the terraces receive a number of adatoms that is proportional to their width, wide terraces complete a given number of rows earlier than narrow ones. The corresponding He intensity oscillations are averaged out as the coverage increases.[15] In Fig. 2, only a faint shoulder is detected at ~ 0.3 ML, the coverage at which the second row is completed. Despite this fact, the He scattering curves still contain information on the surface structure. Apart from the monolayer peak in Fig. 2(a), an intense peak can be observed between 0.5 and 0.6 ML for the two curves. The intensity increase is due to a narrowing of the terrace width distribution during metal deposition with a minimum at 0.5 ML. If no interterrace diffusion occurs, the faster progression of step edges on large terraces and the slower progression on small terraces lead to an averaging of terrace widths between

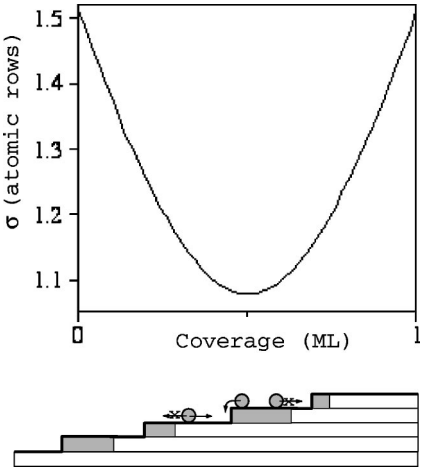

FIG. 3. Simulated terrace width standard deviation σ measured in atomic rows (one atomic row is equal to 2.4 Å) vs adatom coverage. The minimum at 0.5 ML is the result of the adatom confinement effect shown in the scheme at the bottom. The gain in surface periodicity is evident comparing the surface profile before and after deposition of 0.5 ML in the diagram.

neighboring terraces.[31] The reduced deviation from the mean terrace width narrows the He diffraction pattern and increases the peak intensity observed in our measurement. This is further illustrated by a calculation of the terrace width standard deviation for a simple model based on these assumptions, which has been performed over 1000 terraces obeying a Gaussian distribution centered at eight inter-row spacings with a standard deviation of 1.5 rows. The result is displayed in Fig. 3 and it shows that the terrace width distribution goes through a minimum at a coverage of 0.5 ML. As recently shown in a combined TEAS–scanning tunneling microscopy (STM) study,[16] the 0.5-ML peak is observed in the case of Co only between 200 and 290 K and can be directly associated with the formation of straight monolayer wires that cover half the width of a Pt terrace. At $T<200$ K, diffusion processes are too slow for Co adatoms to form regular stripes parallel to the substrate steps. At $T\geqslant 300$ K, Co adatoms have enough thermal energy to diffuse between adjacent terraces, allowing the formation of bilayer islands and thus breaking the periodic pattern of the surface. The presence of the peak at around 0.5 ML (Fig. 2) is therefore an indication of a surface periodic ordering comparable to or even better than that of a clean Pt(997) surface, and it will be used in the following as an indicator for the growth of ordered structures.

B. Growth of Ag/Co wires

We have shown in Sec. II A that by means of TEAS, we can control in real time the step decoration process for Ag and Co separately. We can now take advantage of this fact to deposit a monatomic row along the Pt step edges in order to form a true 1D interface of Co (Ag) atoms. By subsequent deposition of Ag (Co), we can then study how the growth evolves, whether ordered structures will form or intermixing between the two metals will prevent ordering on the atomic scale.

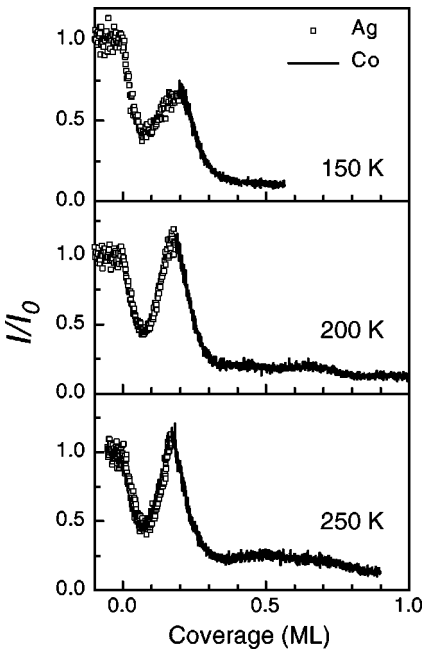

FIG. 4. TEAS reflectivity at $\theta_i = \theta_f = 83°$ as a function of the total coverage of Ag and Co. Deposition of Ag is stopped after completion of a monatomic row and Co is subsequently evaporated on the surface. Ordered growth would result in He intensity maxima during Co deposition, which are not observed in this case.

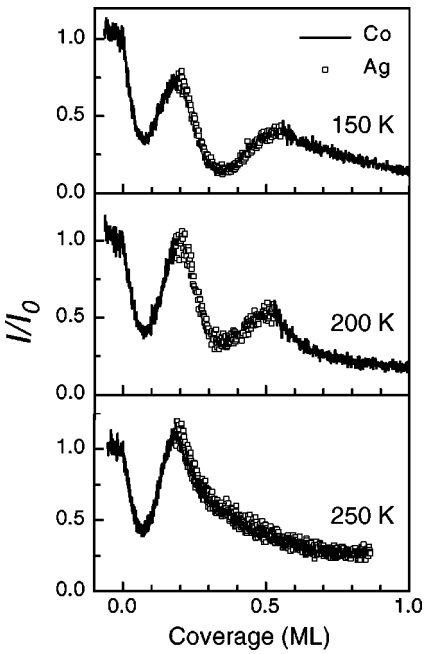

FIG. 5. TEAS reflectivity at $\theta_i = \theta_f = 83°$ as a function of the total coverage of Co and Ag. Ag is deposited after completion of a Co monatomic row; the formation of ordered stripes is inferred at $T = 150$ and $T = 200$ K from the presence of the peak at ~ 0.5 ML.

Figure 4 shows the He reflectivity curves recorded in grazing incidence conditions during subsequent deposition of Ag and Co at 150, 200, and 250 K. First, a monatomic row of Ag has been deposited along each step (peak at ~ 0.17 ML); then Ag deposition has been stopped and after a few seconds we have started evaporating Co. We point out that, if the Co evaporator shutter is kept close, the He beam intensity remains constant after Ag deposition, indicating that no structural changes take place in the Ag row. The monotonic decrease in intensity during Co evaporation shows that the defect density on the surface increases; at 200 and 250 K, we would expect to observe the Co peak at ~ 0.5 ML if Ag and Co formed ordered atomic rows parallel to the Pt step edges. Since this is not the case, we conclude that further row-by-row growth does not take place. The absence of the 0.5-ML peak could be due either to roughening of the step edge or to chemical disorder (Ag/Co intermixing) in the near-step region. Since at $T \geqslant 200$ K the mobility is sufficiently high for both Ag and Co adatoms to rearrange into straight stripes parallel to the Pt steps,[15,16] the missing He beam intensity in the Ag/Co case is likely due to intermixing of the two species. Moreover, the calculations reported in Secs. III D and IV B support this latter point by showing that the structure with a first pure Ag row and a second row filled by Co atoms only (named $Ag^{I}Co^{II}$ for simplicity) is unstable towards alloying. The notation $X^{I}Y^{II}$ will refer in the following to wires consisting of alternated rows of pure metals, where X and Y stand for Ag, Co, and Cu.

We now discuss the reverse situation in which Co is deposited first (Fig. 5). We stop deposition at a coverage corresponding to a Co monatomic row and subsequently start evaporating Ag. At 150 and 200 K, we observe the peak at ~ 0.5 ML, indicating continuous row-by-row growth of Ag on Pt(997).[15] This case is thus different from the previous one as we have indications of ordered structure formation. We suggest that the Co atomic row stays in contact with the Pt steps while the Ag rows align themselves at the Co boundary without considerable intermixing ($Co^{I}Ag^{II}$). This picture is in agreement with the ground-state calculations of the wire atomic structure reported in Secs. III D and IV B. Note that, as the temperature rises, intermixing can occur even in this configuration. In fact, the ~ 0.5-ML peak is not observed in the TEAS curves for $T \geqslant 250$ K. This can be explained by considering that the ground-state energy calculated for an alloyed Ag/Co wire is close to that of the most stable $Co^{I}Ag^{II}$ configuration (see Table IV in Sec. III D).

In Fig. 5, Ag deposition has been stopped at about 0.5 ML and further Co has been deposited on the surface. This was done in order to grow a superlattice with a Co/Ag/Co base, instead of the simple Co/Ag one shown in Fig. 1(a). However, the featureless Co TEAS data reported in Fig. 2(b), as well as in Fig. 5 for coverages larger than 0.5 ML, do not allow us to draw any conclusion on the ordering of such a superlattice.

Surface-confined mixing of Ag and Co has been observed on Ru(0001) (Ref. 23) and on Mo(110).[24] In both cases, intermixing has been attributed to a strain-relief mechanism that compensates for the strain of the opposite sign imposed by the substrate on the two overlayer metals.[32] On Pt(997), as on Ru(0001), Co is under tensile strain while Ag is under compressive strain; however, in contrast to Refs. 23 and 24, such a strain-relief mixing mechanism is unlikely to be at the origin of interdiffusion in our case, at least below 250 K. The

formation of the $Co^{I}Ag^{II}$ structure opposed to the suppression of $Ag^{I}Co^{II}$ cannot be explained in terms of strain since mixing would occur in both cases.

C. Analogy between 1D and 2D Ag/Co growth

A qualitative understanding of the experimental results on the Ag/Co wires can be presented by drawing a parallel between 1D and 2D systems in terms of the interface and surface free energy of Pt, Co, and Ag. It is well known from thin-film epitaxy that layer-by-layer growth with a sharp interface requires a material with a smaller surface free energy to be deposited on a substrate with a higher surface free energy, the interface energy being small to avoid intermixing.[33] If the surface free energy of the deposited material is higher than that of the substrate, segregation can occur. Co has a higher surface free energy when compared to Ag,[34] and Co adatoms on a host Ag surface show a strong tendency to segregate, whereas Ag on a Co surface does not.[35] The above argument holds for 2D films, but our results show that it can be extended to 1D interfaces obtained by step decoration. When Co is evaporated after the deposition of a monatomic Ag row on Pt(997), it ''segregates'' laterally into the Ag row. In the present system, also the stronger tendency of Co to bind to Pt with respect to Ag contributes to the lateral segregation of the Co atoms towards the Pt step. In fact, depending on the adsorption site, we will show in Sec. III that the calculated values of the Co-Pt binding energy are 20–30 % larger than the Ag-Pt one.

To elaborate the analogy between 1D and 2D systems, we have repeated the measurements reported in Fig. 4 and Fig. 5 for Ag and Co monolayer films on Pt(997) instead of monatomic wires. Figure 6 shows the reflected He beam intensity recorded in *nongrazing* conditions during (a) deposition of 1-ML Ag followed by 1-ML Co and (b) deposition of 1-ML Co followed by more than 2-ML Ag. In this scattering geometry, as mentioned in Sec. II, the He reflectivity is determined by the overall surface ordering. At monolayer completion, in the case of layer-by-layer growth, the density of diffuse scatterers is at a minimum, thus resulting in a maximum of the surface reflectivity.[20] Accordingly, the oscillations in Fig. 6 have a period of 1 ML and can be used to calibrate the coverage scale. The relative intensities of the monolayer peaks depend on the corrugation of the He-overlayer potential, on the Debye temperature, and on the ordering of the overlayer.[19] The first peak in Fig. 6(a) corresponds to the formation of a pseudomorphic Ag single layer on the Pt substrate with excellent ordering.[15] The following Co monolayer peak is barely visible, and it is a factor 40 less intense compared to the situation in which Co is deposited first, indicating that the Ag/Co interface is disordered. Reversing the deposition order, we see in Fig. 6(b) that the He beam intensity during Ag evaporation recovers, at monolayer completion, the initial 1-ML Co value and even further oscillations can be detected. We conclude that Ag grows layer by layer on the Co film for the first two layers, as it does on the clean Pt(997) surface.[18]

The $Co^{I}Ag^{II}$ configuration has been shown to be the most stable in the case of decoration of Pt steps by monatomic Co and Ag rows as well as in the case of single monolayer films of Co and Ag on Pt. General thermodynamics arguments commonly applied in the description of thin-film epitaxy can therefore be extended, at least in the present case, to 1D linear interfaces.

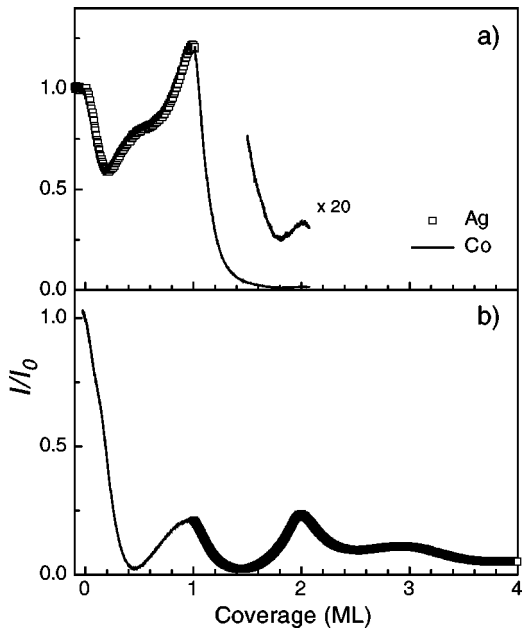

FIG. 6. TEAS reflectivity in nongrazing incidence conditions, $\theta_i = 60.5°$, $\theta_f = 47.2°$. Deposition of 1 ML Ag and subsequently of 1 ML Co at 225 K (a). (b) Same as (a) with reversed order of Ag and Co deposition. In this scattering geometry, the He reflectivity depends on the overall terrace defect density; the TEAS oscillations have a period of 1 ML.

III. CALCULATION OF THE GROUND-STATE ATOMIC STRUCTURE

The calculations reported in this section provide a deeper physical insight into the wire structure and composition in relation with our experimental results. We study the ground-state atomic structure of Ag, Co, and Cu adatoms on Pt(997) by means of a many-body semiempirical potential based on the second moment approximation (SMA). This potential is used to determine first the potential-energy map obtained for a single metal adatom on Pt(997), and then to understand the formation of pure and mixed Co, Ag, and Cu atomic wires along the steps at 0 K. Finally, the wire stability is investigated by means of free-energy calculations at finite temperature.

A. The interaction potential

Many different approaches can be found in the literature to introduce *N*-body interactions, which are required to describe accurately the properties of metals.[36,37] The available methods can be roughly split into two categories. The first one is derived from the density-functional theory and comprises the effective-medium theory (EMT),[38] the embedded-atom method (EAM),[39] and the glue model.[40] These methods are best suited for simple and noble metals. A second cat-

egory of simplified *N*-body potentials has been applied with success to transition metals to explain properties that depend on the effective width of the *d* electronic density of states, determined by its second moment within the tight-binding scheme,[41–47] but not on its details.[37] These potentials are able to account for the cohesive properties of bulk solids,[43] the experimentally observed contraction of the first interlayer spacing occurring at surfaces of transition metals,[37,46] the energy barriers for diffusion,[45] and, to a lesser extent, the elastic constants[43] and the formation energy of a vacancy.[48] Note that beyond empirical and semiempirical potentials, the density-functional theory is able to describe not only the electronic states but also the total energy. At the present time, however, the calculations are too time consuming to be used for large systems.

The potentials based on the second moment approximation (SMA) are probably the most flexible form available in the category of semiempirical potentials since they reasonably describe interactions in transition metals as well as in noble metals (Ag,Au). [42,49] They are written as the sum of site energies E_i that are composed of a repulsive pairwise contribution and a nonadditive attractive part:

$$E_i=(1/2)\sum_{j\neq i} V_{ij}-\Phi\left(\sum_{j\neq i} f_{ij}\right). \tag{1}$$

The attractive part $\Phi(\Sigma_{j\neq i}f_{ij})$ corresponds to the band energy. In the framework of the SMA in the tight-binding scheme, the function $\Phi(x)$ is proportional to x^{α} with $\alpha=\frac{1}{2}$; the attractive f_{ij} and repulsive V_{ij} interactions vary with the interatomic distance r_{ij} according to exponential or power laws. However, it has been proposed[50] that the results derived from a precise tight-binding calculation, i.e., using high-order moments and the local charge-neutrality requirement, are better modeled if the function $\Phi(x)$ is taken to be proportional to $x^{2/3}$, at least when the *d* band is filled with seven electrons per atom, which is the case studied in Ref. 50. Since the exponent α might depend on the *d*-band filling, we will use it as an additional parameter. The repulsive part describes the remainder of the total energy. It is assumed to be pairwise and given by a Born-Mayer potential. The potential energy of the *i*th atom in the presence of its neighbors *j* in a homogeneous system is thus written as

$$E_i=\lambda\sum_j e^{-p[(r_{ij}/r_0)-1]}-\epsilon\left(\sum_j e^{-2q[(r_{ij}/r_0)-1]}\right)^{\alpha}$$

with

$$r_{ij}<r_c. \tag{2}$$

The repulsive (λ,p) and attractive (ϵ,q,α) parameters are obtained by a least mean-square fit of bulk and surface properties of the crystal, namely the experimental values of cohesive energy E_{coh}, bulk modulus *B*, shear elastic constants *C*, and the surface energies of low index surfaces (111), (100), and (110) in cubic crystals.[51,52] r_0 is the nearest-neighbor distance between metal atoms and r_c corresponds to the cutoff distance, which is generally taken to be the second-nearest-neighbor distance to speed up the algorithms. Such a short distance can lead to dramatic effects if we do not impose continuity when $r_{ij}\geqslant r_c$. Therefore, as in Ref. 50, we have to determine the value of the cutoff distance beyond which the parameters do not evolve.

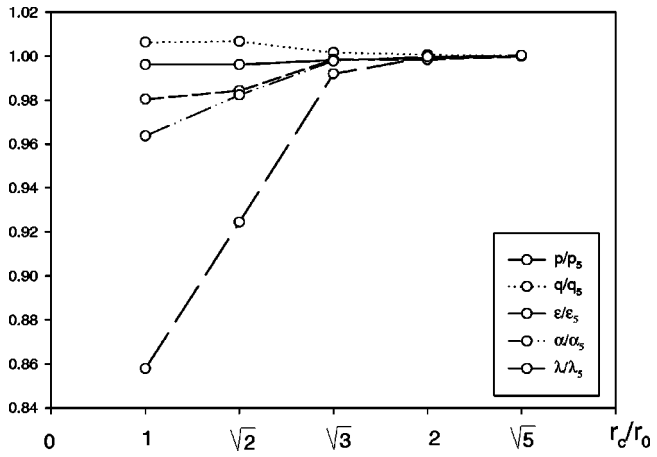

FIG. 7. Dependence of the set of parameters $P_{\mathrm{Pt}}=\{\alpha,p,q,\lambda,\epsilon\}_{\mathrm{Pt}}$ as a function of the cutoff distance r_c reduced by the nearest-neighbor distance r_0 between two Pt atoms. The convergence is optimal when the influence of the fifth nearest neighbors is taken into account.

In Fig. 7, we have drawn the dependence of the set of parameters $P_{\mathrm{Pt}}(\lambda,p,\epsilon,q,\alpha)$ as a function of the cutoff distance r_c. It clearly shows that beyond $2r_0$, all the parameters converge to their values obtained for an infinite cutoff distance r_∞, which is practically attained beyond the fourth neighbors. The same behavior is shown (Fig. 8) for the fitted quantities $F_{\mathrm{Pt}}\equiv\{E_{\mathrm{coh}},B,C,\gamma\}$. The ratios between the best fits and the corresponding experimental values do not change anymore beyond $2r_0$; deviations from unity remain small

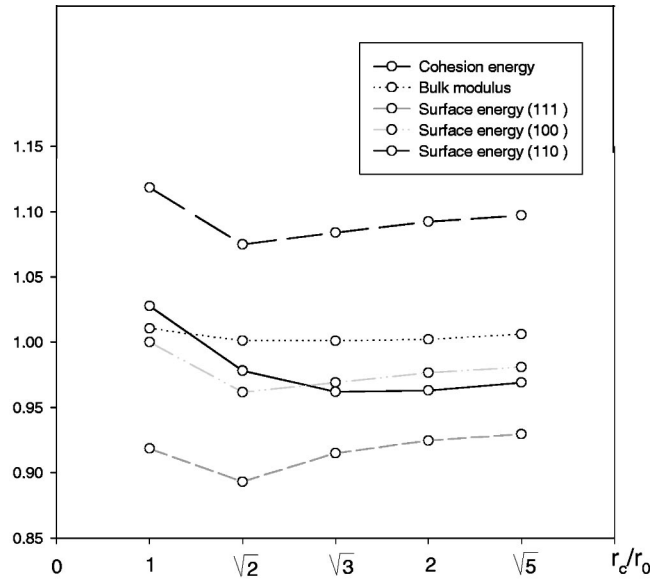

FIG. 8. Ratio between the fitted quantities $F_{\mathrm{Pt}}\equiv\{E_{\mathrm{coh}},B,C,\gamma\}$ and their corresponding experimental values as a function of the cutoff distance r_c reduced by r_0. The ratio does not change anymore beyond $2r_0$.

TABLE I. Potential parameters of Eq. (2) for the different adsorbed species.

	Pt	Co	Cu	Ag
r_0 (Å)	2.77	2.51	2.55	2.89
λ (eV)	2.9135	0.2361	0.7776	1.9994
p	6.9662	8.2732	5.9935	6.2177
ϵ (eV)	3.9653	0.7918	1.2952	2.5096
q	3.2087	1.8493	2.4055	2.9138
α	0.93365	0.8570	0.9097	0.9518

(less than 8%) for most of the observables F_{Pt} and are much smaller than the deviations obtained by using the standard values $\alpha=\frac{1}{2}$ and $r_c=\sqrt{2}r_0$, especially for the surface energies. The maximum discrepancy occurs for the elastic constants ($\leqslant 30\%$), for which a perfect agreement is not expected since the potential depends only on the interatomic distances and not explicitly on the angular deformations. The optimized values of the potential parameters are given in Table I for Pt, Co, Ag, and Cu. Remarkably, the parameter α remains close to unity ($\alpha \simeq 0.8-0.9$) for most species, indicating that the potential in Eq. (2) is not far from being pairwise. Nevertheless, it would be an error to consider that metals could be modeled by strictly pairwise potentials since the observed inward relaxation of the surface planes of the metal cannot be explained with $\alpha=1$.

The generalization of Eq. (2) to the case of heteroatomic systems is not straightforward, especially due to the exponent α, which, contrary to the usual SMA, is not the same for all metals. We have tried several ways to overcome this problem and we have found comparable results within an uncertainty of 10%. Here we take α_X for X-X interactions and α_{Pt} for the X-Pt interactions. This assumption is not crucial since all the α parameters are quite close to each other ($\alpha=0.9\pm0.05$). As is usually done with the second moment potential, we have used arithmetic averages for the distances r_0 and r_c and geometric averages for the parameters p, q, λ, and ϵ. The contribution to the binding energy arising from the perturbation of the substrate has been evaluated to be less than 15% and thus neglected. The contribution of this term to the variation of the adsorption energies as a function of the atomic environment, which are the relevant quantities in our problem, is even smaller. In the following, all the adsorption energies are defined as the energy difference between the substrate with the adsorbates and the clean substrate plus the adatoms in the free state.

B. Potential-energy map for a single metal atom on the Pt(997) surface

We determine the equilibrium adsorption site of a single adatom on the stepped platinum surface in order first to evaluate the adatom potential energies and its corrugation, and then to discuss the influence of steps when compared to the flat surface. This can be done by drawing the adatom potential energy map obtained as follows: The potential energy E_i of the adatom at the position $\mathbf{r}_i$ (x_i,y_i,z_i) is minimized with respect to z_i for a given lateral position (x_i,y_i) and the value of the minimum $E_i^{\min}$ is plotted as a function of (x_i,y_i). A typical energy map obtained for Co on Pt(997) is drawn in Fig. 9; the other adsorbates would give similar shapes. Four main quantities characterize the map and are required to model the adsorption of a metal atom on a vicinal surface: the potential well depth of the stable adsorption sites ΔE_T and the corrugation energy ΔE between two stable sites along the diffusion valley on a terrace, the depth of the adsorption well ΔE_S at the bottom of the step edge, and the so-called Ehrlich-Schwoebel barrier ΔH_S at the step, i.e., the additional activation barrier for an adatom to jump down at a step edge.

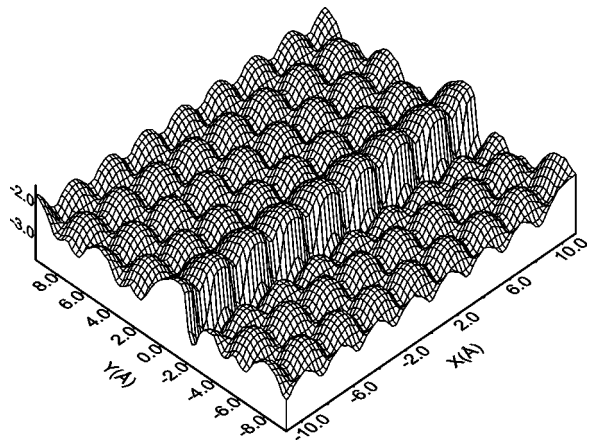

FIG. 9. Potential-energy map (in eV) experienced by a Co adatom above the Pt(997) surface. The step is parallel to the X axis.

Table II gives the values of these four quantities for the Co, Cu, and Ag adsorbates. The stable sites on the terrace and at the step are the hollow sites with an adsorption well significantly lower at the step since the ratio $\Delta E_S/\Delta E_T$ is equal to 1.4. This value is obviously related to the larger adatom coordination at step sites.[53] As expected, the largest values of ΔE_S and ΔE_T are obtained for Co while the corresponding quantities for Cu and Ag are similar and appreciably smaller since in the latter metals the d band is filled and thus its contribution to the cohesive properties almost vanishes. The same behavior is obtained for the corrugation ΔE above the terrace and for ΔH_S. These data indicate that the Co adatoms should be strongly trapped in the terrace and step adsorption sites compared to Cu and Ag, which should diffuse more easily.

TABLE II. Adsorption energy (in eV) of a single metal atom above the Pt(997) surface derived from the calculation of the potential-energy maps.

	Co/Pt	Cu/Pt	Ag/Pt
ΔE_T	-2.79	-2.17	-2.14
ΔE_S	-3.79	-2.75	-2.68
ΔE	0.26	0.17	0.14 (0.17)[a]
ΔH_S	0.59	0.46	0.39

[a]Experimental value from Ref. 56.

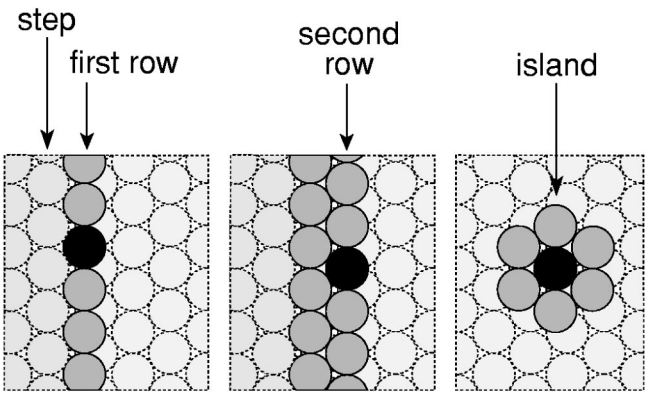

FIG. 10. Schematic representation of different geometries for which the energy of the adatom (black circle) is calculated. The corresponding energies are listed in Table III.

C. Structure of metal adatoms on Pt(997): Pure Co, Ag, and Cu wires

In line with the experiment (Sec. II A), we start by analyzing the structure of pure Co, Ag, and Cu wires. We determine the minimum potential energy of a set of N metal atoms adsorbed on a terrace of the stepped metal surface of platinum. The Pt substrate is assumed to be rigid and the steps are perfectly linear (without kinks). The minimum search is performed at 0 K using a numerical conjugate-gradient procedure.

1. Co

The lattice parameter of bulk Co (2.50 Å) is smaller than the parameter of bulk Pt (2.77 Å). Despite this large misfit, our calculations show that large (400 atoms) 2D islands on Pt(111) have a commensurate (1×1) structure in registry with the substrate. The Co atoms occupy the hollow sites of the substrate. The same site occupations are obtained in the presence of a monatomic step since its influence remains short range. Table II shows that the adsorption energy for a single Co adatom in the first row of sites along the Pt steps is -3.79 eV while it increases to -2.86 eV in the second row, close to the value of the adsorption energy on the terrace (-2.79 eV).

At intermediate Co coverage on the terrace, the analysis of the potential energy can give information on the possible growth mechanism. Because of the deep potential well viewed by a single Co atom at the bottom of the Pt step, the energy minimization at 0 K leads to the formation of a Co row located at the lower terrace and oriented parallel to the step edge. The interatomic distance between the Co atoms is equal to the distance between adjacent Pt hollow sites. These results agree well with a previous STM study of Co/Pt(997).[16] The energy per Co atom in this completely filled first row (Fig. 10) is equal to -4.20 eV. Examination of the data given in Table III shows that the energy per adatom in the second complete row increases significantly to -3.38 eV, a value that is slightly larger than the mean energy of the same adatom embedded in an island on the terrace (-3.48 eV). This indicates, from a strict interpretation of the data at 0 K, that the configuration corresponding to the formation of the second row is less stable than the corresponding formation energy (per atom) of a very large island on the terrace.

2. Ag

Unlike Co, Ag has a lattice parameter (2.89 Å) that is slightly larger than that of Pt. The geometry above a terrace is still (1×1), with the Ag atoms occupying the Pt hollow sites. At the step, Ag forms a complete first row with adsorption energy equal to -3.15 eV per atom (Fig. 10). The adsorption energy increases in the second filled row to -2.80 eV. This value is the same as the corresponding energy per atom in a very large island (Table III). Hence, at 0 K the second row formation is as stable as the formation of Ag islands on the terrace.

3. Cu

The lattice parameter of bulk Cu (2.55 Å) is smaller than the corresponding value for Pt(111). The mean adsorption energy per Cu atom embedded in a Cu island is equal to -2.77 eV in the stable hollow site of the Pt terrace. At the step edge, the adsorption energy per atom in the first filled row (-3.12 eV) is appreciably lower than the value corresponding to a Cu atom in the second row (-2.71 eV). This latter energy is higher than the adsorption energy per atom in a large island, leading to a better stability for the island than for the second row formation (Table III).

To summarize this section, the formation of a row of Co, Ag, and Cu adatoms close to the Pt step is always energetically favored, indicating the possibility of growing 1D monatomic wires on the vicinal Pt(997) surface. In the experiments (Sec. II and Refs. 15 and 16), 1D wires are indeed obtained by self-organization, provided that the substrate temperature allows for sufficiently fast diffusion of the adatoms. On the basis of thermodynamic arguments, since the influence of the step is short range, we would expect a strong competition at equilibrium between the formation of a second wire parallel to the step and the aggregation of adatoms in large 2D islands on the terraces. On Pt(997), however, the growth of large 2D islands (where most adatoms have monolayerlike coordination) cannot take place due to the small width of the terraces. Kinetic effects will further increase the tendency for row-by-row growth. Experimentally, we find that the formation of 2D islands detached from the steps does not indeed take place. Given the small width of the Pt(997) terraces compared to the average diffusion length of a monomer at $T\gtrsim100$ K, adatoms readily migrate and attach to the step edges prior to nucleate on the terraces.[15]

TABLE III. Adsorption energy (eV) per adatom on Pt(997) as a function of its position with respect to the step and on the terrace.

	First row	Second row	Large island
Co	-4.20	-3.38	-3.48
Ag	-3.15	-2.80	-2.80
Cu	-3.12	-2.71	-2.77

D. Structure of metal adatoms on Pt(997): Ag/Co and Co/Cu wires

We report here the results of the ground-state calculation of the structure of Ag/Co and Co/Cu wires. A preliminary comparison (without taking temperature effects into account) can be made with the experimental results obtained for Ag/Co (Sec. II B). In particular, we intend to explain why the self-organized growth of $Co^{I}Ag^{II}$ wires is favored over $Ag^{I}Co^{II}$. We consider an equimolar mixture of atoms of two different metals adsorbed on the Pt(997) surface. The minimum energy search has been performed according to the same numerical conjugate-gradient procedure. A set of $N/2$ atoms of the A species and $N/2$ atoms of the B species is adsorbed along the step of the Pt(997) surface and the minimum energy is determined for every arrangement of A and B species in the sites. The calculations are presented for $N=16$, the Pt(997) terrace comprising two atomic rows with eight atoms each. Periodic boundary conditions are applied along the row to eliminate edge effects.

1. Ag/Co wires

The potential-energy values corresponding to different arrangements of Ag and Co atoms are reported in Table IV. The most stable structure is obtained when Co atoms occupy the first row close to the step and Ag atoms occupy the second row. Such a structure is labeled $Co^{I}Ag^{II}$ in analogy with the nomenclature used in the experimental part (Sec. II B). The least stable geometry corresponds to the case in which the first row sites are occupied by Ag atoms while Co atoms occupy the second row sites ($Ag^{I}Co^{II}$ structure). These results agree well with the He scattering data presented in Sec. II B, which show that ordered $Co^{I}Ag^{II}$ wires form when Co is deposited first and Ag second on Pt(997) at $T \leqslant 200$ K.

All the other configurations in which the Co and Ag atoms lie randomly within the first two rows close to the step edges lead to intermediate adsorption energies. These results indicate that the Co atoms prefer to coat the Pt step, a situation for which the interactions between Pt and Co are optimized. The reverse situation occurs for Ag, which is less ''attracted'' by the step and allows the Co to be closer to the step. The interactions between Ag atoms, Co atoms, and between Ag and Co atoms are very similar and do not provide selectivity in the random or ordered lateral arrangements of the binary mixture. As a result, intermediate structures with Co and Ag adatoms in both the first and second row are favored with respect to $Ag^{I}Co^{II}$ when Ag is deposited first, close to the step.

2. Co/Cu wires

A similar situation occurs for the binary mixture of Cu and Co atoms. The most stable structure corresponds to a first row of cobalt atoms that coat the step and to a second row formed by Cu atoms ($Co^{I}Cu^{II}$). The potential energy of the reverse structure ($Cu^{I}Co^{II}$) is clearly larger (Table IV). The energy difference between $Co^{I}Cu^{II}$ and alloyed Co/Cu rows is larger compared to that between Co^{I} Ag^{II} and alloyed Ag/Co rows. The stronger tendency of Ag to arrange close to the step edge with Co atoms in order to form an alloy is due to the fact that Ag atoms are more strongly bound to the Pt step than Cu atoms.

TABLE IV. Total energy (in eV) of equimolar Ag/Co and Co/Cu mixtures. The energy values are calculated for a system formed by eight Co atoms and eight Ag (or eight Cu) atoms, which are restricted to occupying the first two rows closest to the lower step edge. Four types of atomic configurations are considered (X = Ag or Cu): $Co^{I}X^{II}$ when the Co atoms and X atoms occupy the first and second row, respectively; Co X ordered alloy; Co X disordered alloy (an average has been performed over many configurations); $X^{I}Co^{II}$, where the X atoms and the Co atoms occupy the first and second row, respectively.

	$Co^{I}Ag^{II}$	Ag/Co ordered alloy	Ag/Co disordered alloy	$Ag^{I}Co^{II}$
E	−62.44	−62.26	−61.15	−58.86
	$Co^{I}Cu^{II}$	Co/Cu ordered alloy	Co/Cu disordered alloy	$Cu^{I}Co^{II}$
E	−60.22	−58.66	−57.97	−57.26

IV. STABILITY OF BINARY COMPOSITION WIRES AT FINITE TEMPERATURE

To get a more reliable comparison between experiment and theory, we need to include temperature effects into our model in order to study the stability of wires containing two adatom species (A and B). Moreover, we want to clarify how the experimental preparation, and more precisely the initial choice of deposition (A deposited before or after B), influences the alloying process. We are aware that the experimental conditions described in Sec. II do not necessarily correspond to a model based on equilibrium thermodynamics and that growth could also be determined by out-of-equilibrium processes. However, three main reasons justify the development of a thermodynamic approach based on the Ising model in the present case. First, kinetic effects will play only a minor role in the formation of an alloyed phase, since species A has already reached a thermodynamically stable state before the deposition of species B begins. Second, the results of thermodynamics are often qualitatively informative of the situations that appear in the growth model. Third, the time interval between two successive depositions (~ 10 s) is much longer than typical surface diffusion processes. The experimental conditions should be close to a regime of thermodynamic quasiequilibrium.

A. Ising model for binary alloy wires

We consider a mixture of two metal atom species A and B adsorbed at temperature T on a Pt(997) terrace containing $(L \times N)$ adsorption sites, where L is the number of rows that can be formed parallel to the step and N is the number of sites inside a row. The occupation of the nth site belonging to the lth row, denoted as the (l,n)th site ($1 \leqslant l \leqslant L$, $1 \leqslant n \leqslant N$), is described by σ_{ln}, which is equal to 1 or 0 according to whether the site is occupied or not, whereas $S_{ln} = -1$ or $+1$ characterizes the atom type (A or B, respectively) at the (l,n)th site.

The Ising Hamiltonian H for a binary alloy is written in the pairwise and nearest-neighbor interaction approximations as

$$H=-\sum_{l,n}\left[\left(\frac{2\mu(l)-V_{A\text{-Pt}}(l)-V_{B\text{-Pt}}(l)}{2}\right)\sigma_{ln}+\left(\frac{V_{A\text{-Pt}}(l)-V_{B\text{-Pt}}(l)}{2}\right)\sigma_{ln}S_{ln}\right]+\tfrac{1}{2}\sum_{l,n}\sum_{l',n'}\left[\left(\frac{V_{AA}+V_{BB}+2V_{AB}}{4}\right)\sigma_{ln}\sigma_{l'n'}-\left(\frac{V_{AA}-V_{BB}}{4}\right)(S_{ln}+S_{l'n'})\sigma_{ln}\sigma_{l'n'}+\left(\frac{V_{AA}+V_{BB}-2V_{AB}}{4}\right)\sigma_{ln}S_{ln}\sigma_{l'n'}S_{l'n'}\right], \quad (3)$$

where $V_{A\text{-Pt}}(l)$ and $V_{B\text{-Pt}}(l)$ define the holding interaction between an adatom (A or B) in the lth row and the Pt substrate atom. V_{AA}, V_{BB}, and V_{AB} are the pairwise energies between adatoms, and $\mu(l)$ is the chemical potential for the lth row at equilibrium. Note that the potential parameters occurring here cannot be precisely known since such a separation in pairwise contributions (bond-breaking model[54]) is not accurate due to the natural nonadditivity of the metallic interactions. Nevertheless, it gives some indications of the physical processes, and when the mean-field approach is used, within this pairwise approximation, the free energy can be readily calculated.

In fact, the model becomes analytically tractable (cf. Appendix A) when we limit our analysis to three rows completely filled by an equimolar mixture of atoms A and B interacting with a similar lateral potential $V_{AA}=V_{BB}$. The free energy per adatom is then written as

$$\frac{F}{N}=\frac{F}{N}(0)+\{[b(3)-b(1)]M_1+[b(3)-b(2)]M_2+2\eta M_1(M_1+M_2)\}+k_BTf(M_1,M_2). \quad (4)$$

F/N is a function of two independent order parameters M_1 and M_2 that represent the molar fraction of adatoms A (or adatoms B) in the first or second row, respectively. $(F/N)(0)$ is a scale factor that depends on the holding contribution $V_{A\text{-Pt}}(l)$ and $V_{B\text{-Pt}}(l)$ and on the lateral terms V_{AA}, V_{BB}, and V_{AB} (cf. Appendix A). The term $b(l)$ is the potential-energy difference between $V_{A\text{-Pt}}(l)$ and $V_{B\text{-Pt}}(l)$ in the lth row, which characterizes the potential increment of the adatom-step interaction in the successive rows (cf. Fig. 9). The term η describes the difference between homointeractions (V_{AA} and V_{BB}) and heterointeractions (V_{AB}) and plays the dominant role in mechanisms leading to the order/disorder phase transition.

The values of the various parameters occurring in Eq. (4) for the three metal species (Co, Ag, and Cu) can be extracted from Table III data and they have been already discussed in Sec. III C. The solutions leading to minima for F/N in Eq. (4) can be discussed in a more general way by drawing the reduced free-energy map per adatom $F^*/N=F/Nk_BT$ as a function of M_1 and M_2 for various values of parameters η^* and $b(1)^*,b(2)^*,b(3)^*$ reduced by the thermal energy k_BT. Since $b(2)^*\simeq b(3)^*$, due to the short-range influence of the step, the significant parameters are $b(1)^*-b(3)^*$ and η^*. The solutions of Eq. (4) are therefore discussed in terms of these two coefficients for the Ag/Co, Co/Cu, and Ag/Cu mixtures.

B. Stability of Ag/Co wires

To allow an easier interpretation of the finite-temperature results, we plot the free energy per adatom as a function of the molar fractions of A and B atoms in the first two rows along a step, M_1 and M_2, respectively. This is done in Fig. 11(a) for $T=220$ K and $b(1)^*-b(3)^*=30$, which is a value characteristic of the Ag/Co system, to enable a comparison with the experimental data of Sec. II B. For small values of η^*, the lowest free energy (-500 meV) is obtained when $M_1=1$ and $M_2=-1$, showing that the first row is fully occupied by Co atoms while the second row contains the Ag species. Note that the isoenergetic sampling is less narrow along M_2, indicating that the second row can also contain a small fraction of Co atoms and form an Ag/Co alloy. When η^* increases up to 20, two minima occur. In the deepest potential well (-540 meV), the first row is formed mainly by Co atoms ($M_1=0.9$) while the second row contains Ag atoms only ($M_2=-1$). The other well (-40 meV) corresponds to a situation in which the first row is occupied by an alloy of Ag and Co atoms ($M_1=-0.15$) with a slightly larger fraction of Ag atoms, while the second row is filled by Co atoms only ($M_2=1$). For still larger η^* values, the aforementioned effect is enhanced. The deepest well (-800 meV) corresponds to an alloy Ag/Co in the first row preferentially composed by Co atoms ($M_1=0.5$) while the second row is filled by Ag atoms ($M_2=-1$). The second energy minimum (-300 meV) occurs for $M_1=-0.25$ and $M_2=1$, i.e., for a disordered first row filled by a Ag/Co alloy and a second Co row. From these results, we conclude that the formation of a first Ag row (Ag^ICo^{II}) is clearly less favorable for any η^* values.

The value of η^* calculated from the potential [Eq. (2)] for the equimolar Ag/Co system is equal to 12. This value is probably underestimated due to the use of an effective pairwise interaction model for its calculation. The calculated value of η^* leads to the stability of a first Co row consistent with the map drawn in the middle of Fig. 11(a). The ordering process can be summarized as follows. When Co is deposited first, it forms a very stable Co row at the step edge; subsequent addition of Ag atoms completes the second row. This is the Co^IAg^{II} configuration found in the experimental part. By contrast, when Ag is deposited first, unphysical values of η^* would be required to prevent the Co atoms from occupying the first row at the expense of Ag atoms. The Ag^ICo^{II} structure cannot be stabilized and the system directly forms an alloy, because no energy barrier separates the Ag^ICo^{II} phase from the mixed phase, in agreement with the experimental findings obtained in Sec. II B. The transition from the alloy towards the stable $Co^I Ag^{II}$ ordering is also possible since the two energy minima are separated by a

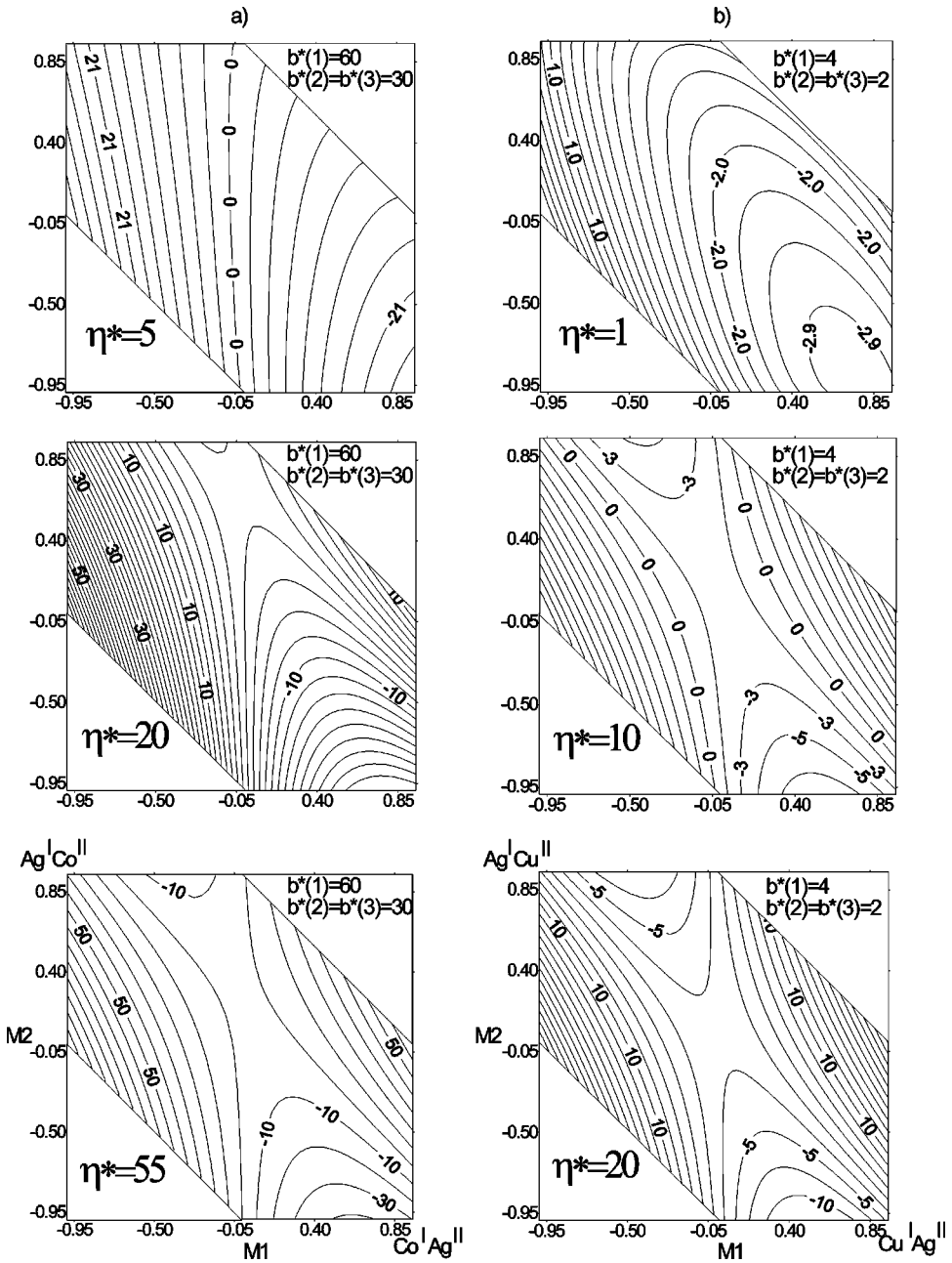

FIG. 11. Reduced free-energy maps as a function of the molar fractions M_1 and M_2 of metal atoms in the first and second row. The values of $b(1)^*$, $b(2)^*$, $b(3)^*$, and η^* potential parameters are given in each map. Column (a) corresponds to situations relevant for the Ag/Co and Co/Cu systems and column (b) characterizes rather the Ag/Cu case. $M_l=0$ corresponds to a binary alloy of A and B species, $M_l=\pm 1$ to pure A or B wires, as indicated at the bottom of the two columns.

barrier of 30 meV while the reverse path from $Co^{I}Ag^{II}$ towards the alloy is forbidden due to a barrier height of 700 meV.

C. Stability of Co/Cu and Ag/Cu wires

A better understanding of the results obtained for the Ag/Co system can be gained by making a comparison with other species that were not investigated experimentally in this paper. Moreover, we can clarify here the role of the two main parameters $b(1)^*-b(3)^*$ and η^* on the self-organized growth of binary alloy wires.

A behavior similar to Ag/Co is expected for Co/Cu wires on the basis of similar values for $b(1)^*-b(3)^*$ for this mixture (see Table III). We thus refer to Fig. 11(a) to discuss the Co/Cu wires. The calculated η^* value for Co/Cu is $\eta^*=3$, about four times smaller than the value obtained for the Ag/Co system. By looking at Fig. 11(a) (top), we see that the deposition of Co atoms would lead to the formation of a very stable first row of pure Co ($M_1=1$) without mixing with additional Cu atoms, these latter forming the second row ($M_2=-1$), i.e., a situation corresponding to $Co^{I}Cu^{II}$. When Cu is deposited first, the formation of the $Cu^{I}Co^{II}$ structure is unstable with respect to the alloy ($M_1=M_2=0$) and clearly much less stable than the $Co^{I}Cu^{II}$ structure.

The Ag/Cu mixture is characterized by smaller values of $b(1)^*$, $b(3)^*$, and η^* when compared to the Ag/Co and Co/Cu mixtures. We see in Fig. 11(b) that for very small values of η^* ($\eta^*=1$), the first row is mainly filled by Cu atoms while the Ag atoms occupy the second row. However, a small fraction of the other species can be present in both rows, leading to the formation of a Ag/Cu alloy in the first

two rows with a dominant species ($M_1=0.85, M_2=-0.70$). When η^* increases up to 10, two minima occur. The first one at -170 meV, obtained for $M_1=0.5$ and $M_2=-1$, corresponds to the main occupation of the first row by Cu atoms while the second row is fully occupied by Ag atoms. The second minimum is slightly less deep (-100 meV) and it occurs for $M_1=-0.3$ and $M_2=1$, i.e., as the first row is formed by a Ag/Cu alloy while the second row is occupied by Cu. For significantly larger values of η^* ($\eta^*=20$), the two previous minima tend to become equivalent with a barrier roughly equal to 170 meV. In the first minimum, the first row is mainly filled by Cu atoms ($M_1=0.5$) and the second row by Ag atoms ($M_2=-1$) forming the $Cu^{I}Ag^{II}$ structure. The reverse situation occurs in the second minimum.

The estimated value of η^* for the Ag/Cu system [Eq. (2)] is equal to 5 and corresponds approximately to the middle map in Fig. 11(b). In this case, when Cu is deposited first on the surface, it forms an ordered row at the step that is not destroyed by the addition of Ag atoms. The latter species arranges itself in a complete second row. The reverse situation $Ag^{I}Cu^{II}$ can also be obtained even if this peculiar ordering does not correspond to the most stable situation. In fact, when Ag atoms are deposited first, the system can freeze in the metastable $Ag^{I}Cu^{II}$ structure corresponding to the second well since the alloy is clearly less stable and because the high-energy barrier that traps the system in this state prevents it from reaching its minimum configuration $Cu^{I}Ag^{II}$.

The features deduced from this thermodynamic model are qualitatively in good agreement with the experimental data concerning the growth of binary Ag/Co wires. In particular, we have evidenced that $Co^{I}Ag^{II}$ is the most stable structure and that, conversely, $Ag^{I}Co^{II}$ is unstable towards alloying. The analysis of the Co/Cu and Ag/Cu systems cannot be supported at present by experimental evidence. We have shown that the formation of two wires of different composition can be obtained for particular values of the main parameters η^* and $b(1)^*-b(3)^*$. We point out that a detailed understanding and predictive analysis of epitaxial binary alloy growth rest on an accurate description of the metal/metal interaction potentials.

V. CONCLUSIONS

In the present paper, we have investigated the formation and thermodynamic stability of bimetallic wires obtained by step decoration of Pt vicinal surfaces. Sequential deposition of Ag and Co on Pt(997) has been investigated by TEAS as a means to obtain a periodic array of wires formed by alternated Ag and Co monatomic chains. When a monatomic Co row is deposited first and is in contact with the Pt edge atoms, subsequent Ag deposition at 150 K$\leqslant T\leqslant$200 K leads to the formation of compositionally ordered Co/Ag stripes parallel to the Pt steps ($Co^{I}Ag^{II}$). In contrast, atomic chains of mixed composition are obtained when Ag is deposited before Co. Calculations based on semiempirical potentials agree with the experimental data, showing that the equilibrium configuration of a binary Ag/Co wire determined at 0 K corresponds to the first row filled by Co and the second row by pure Ag. The results of the thermodynamic approach developed at finite temperature corroborate the stability of the $Co^{I}Ag^{II}$ configuration and show that the reverse structure $Ag^{I}Co^{II}$ is clearly unstable, leading to the occurrence of an Ag/Co alloy in the first two rows along the steps. In addition, calculations have been extended to Co/Cu and Ag/Cu binary mixtures in order to stimulate experiments not available to date and to test the predictive character of the present numerical approach.

APPENDIX: FREE ENERGY OF THE BINARY ALLOY

When the mean-field approach is used, the Ising Hamiltonian defined in Eq. (3) can be rewritten as

$$\begin{aligned}\bar{H}=\sum_{l,n}\Bigg[&[-\mu(l)+B(l)-b(l)S_{ln}]\sigma_{ln}+2\gamma\left(\sigma_{ln}-\frac{\theta_l}{2}\right)\Theta_l\\&-2\delta\left(S_{ln}\sigma_{ln}-\frac{M_l}{2}\right)\Theta_l-2\delta\left(\sigma_{ln}-\frac{\theta_l}{2}\right)\Pi_l\\&+2\eta\left(\sigma_{ln}S_{ln}-\frac{M_l}{2}\right)\Pi_l\Bigg],\end{aligned}\tag{A1}$$

where the potential coefficients appearing in Eq. (A1) are defined as

$$\begin{aligned}B(l)&=\tfrac{1}{2}[V_{A\text{-}\mathrm{Pt}}(l)+V_{B\text{-}\mathrm{Pt}}(l)],\\b(l)&=\tfrac{1}{2}[V_{A\text{-}\mathrm{Pt}}(l)-V_{B\text{-}\mathrm{Pt}}(l)],\\\gamma&=\frac{V_{AA}+V_{BB}+2V_{AB}}{4},\\\delta&=\frac{V_{AA}-V_{BB}}{4},\\\eta&=\frac{V_{AA}+V_{BB}-2V_{AB}}{4}.\end{aligned}\tag{A2}$$

In the particular geometry studied here, an adatom in a given row l ($l\neq 1,L$) has two nearest neighbors in its own row as well as in the two adjacent rows. The mean occupation θ_l of the lth row parallel to the step is expressed as

$$\theta_l=\langle\sigma_{ln}\rangle\tag{A3}$$

and M_l is the difference between θ_l^B and θ_l^A of row l in atoms B and A, respectively,

$$\begin{aligned}\theta_l^A&=\left\langle\sigma_{ln}\left(\frac{1-S_{ln}}{2}\right)\right\rangle,\\\theta_l^B&=\left\langle\sigma_{ln}\left(\frac{1+S_{ln}}{2}\right)\right\rangle,\\M_l&=\langle\sigma_{ln}S_{ln}\rangle=\theta_l^B-\theta_l^A,\end{aligned}\tag{A4}$$

where $\langle\cdots\rangle$ means a statistical average over the canonical distribution. Finally,

$$\begin{aligned}\Theta_l&=\sum_{l'}^{l+1}{}_{l-1}\,\theta_{l'},\\\Pi_l&=\sum_{l'}M_{l'},\end{aligned}\tag{A5}$$

and $\Theta_1=\theta_1+\theta_2$, $\Theta_L=\theta_{L-1}+\theta_L$, $\Pi_1=M_1+M_2$, $\Pi_L=M_{L-1}+M_L$.

The free energy is readily obtained from Eq. (4.18a) of Ref. 55 applied to the case of a ''ternary'' alloy made of A and B atoms plus vacancies,

$$F=N\sum_l [-\mu(l)+B(l)]\theta_l-b(l)M_l+\gamma\theta_l\Theta_l-\delta M_l\Theta_l - \delta\theta_l\Pi_l+\eta M_l\Pi_l+k_BT\left[\frac{\theta_l-M_l}{2}\ln\left(\frac{\theta_l-M_l}{2}\right) + \frac{\theta_l+M_l}{2}\ln\left(\frac{\theta_l+M_l}{2}\right)+(1-\theta_l)\ln(1-\theta_l)\right] \tag{A6}$$

Such an energy depends on the chemical potential μ, on the temperature T through $\beta=(kT)^{-1}$, and on the various potential parameters and statistical quantities. The complete analysis of the growth mode cannot be readily carried out since it requires the study of the function $F(l)$ versus all the parameters involved.

Here we limit our analysis to the growth of three rows completely filled by an equimolar binary mixture of atoms A and B interacting through very similar lateral interaction potentials $V_{AA}\simeq V_{BB}$. As a result, the number of atoms A and B is fixed, the potential coefficient δ vanishes, and the number of degrees of freedom decreases due to the constraints imposed on the θ_l and M_l values. Indeed, the completion of the three rows requires that $\theta_1=\theta_2=\theta_3=1$, leading to the additional conditions $\Theta_1=\Theta_3=2$ and $\Theta_2=3$. Moreover, for a binary mixture, the condition $M_1+M_2+M_3=0$ must necessarily hold, implying the additional expressions $\Pi_1=M_1+M_2$, $\Pi_2=0$, and $\Pi_3=-M_1$.

Within these assumptions, the free energy per adatom depends only on the two order parameters M_1 and M_2 instead of the 14 independent degrees of freedom θ_l and M_l ($l=1,\ldots,8$). The third row behaves as an atom bath that supplies metal atoms A or B to the first two rows, in order to reach thermodynamic equilibrium. The free energy is thus written as a sum of three contributions, as

$$\frac{F}{N}=\frac{F}{N}(0)+\{[b(3)-b(1)]M_1+[b(3)-b(2)]M_2 + 2\eta M_1(M_1+M_2)\}+k_BTf(M_1,M_2). \tag{A7}$$

$(F/N)(0)$ appears as a scale factor defined as

$$\frac{F}{N}(0)=B(1)+B(2)+B(3)+7\gamma, \tag{A8}$$

while the two other contributions depend on M_1 and M_2. The second contribution mixes M_1,M_2 and the potential coefficients, while the third term $f(M_1,M_2)$ is a function of M_1 and M_2 only, defined as

$$f(M_1,M_2)=\frac{1-M_1}{2}\ln\left(\frac{1-M_1}{2}\right)+\frac{1+M_1}{2}\ln\left(\frac{1+M_1}{2}\right) + \frac{1-M_2}{2}\ln\left(\frac{1-M_2}{2}\right)+\frac{1+M_2}{2}\ln\left(\frac{1+M_2}{2}\right) + \frac{1-M_1-M_2}{2}\ln\left(\frac{1-M_1-M_2}{2}\right) + \frac{1+M_1+M_2}{2}\ln\left(\frac{1+M_1+M_2}{2}\right). \tag{A9}$$

[1] J. A. Rodriguez, Surf. Sci. Rep. **24**, 223 (1996).

[2] F. J. Himpsel, J. E. Ortega, G. J. Mankey, and R. F. Willis, Adv. Phys. **47**, 511 (1998), and references therein.

[3] B. Újfalussy, L. Szunyogh, P. Bruno, and P. Weinberger, Phys. Rev. Lett. **77**, 1805 (1996).

[4] C. H. Lee, R. F. C. Farrow, C. J. Lin, E. E. Marinero, and C. J. Chien, Phys. Rev. B **42**, 11 384 (1990).

[5] G. H. O. Daalderop, P. J. Kelly, and M. F. H. Schuurmans, Phys. Rev. B **44**, 12 054 (1991).

[6] J. Thiele, C. Boeglin, K. Hricovini, and F. Chevrier, Phys. Rev. B **53**, R11 934 (1996).

[7] E. E. Fullerton, D. M. Kelly, J. Guimpel, I. K. Schuller, and Y. Bruynseraede, Phys. Rev. Lett. **68**, 859 (1992).

[8] P. Beliën, R. Schad, C. D. Potter, G. Verbanck, V. V. Moshchalkov, and Y. Bruynseraede, Phys. Rev. B **50**, 9957 (1994).

[9] W. C. Chiang, W. P. Pratt, M. Herrold, and D. V. Baxter, Phys. Rev. B **58**, 5602 (1998), and references therein.

[10] R. Schad, P. Beliën, G. Verbanck, V. V. Moshchalkov, Y. Bruynseraede, H. E. Fischer, S. Fischer, and M. Bessiere, Phys. Rev. B **59**, 1242 (1999).

[11] W. P. Pratt, S. F. Lee, J. M. Slaughter, R. Loloee, P. A. Schroeder, and J. Bass, Phys. Rev. Lett. **66**, 3060 (1991).

[12] T. Kingetsu, J. Appl. Phys. **76**, 4267 (1994).

[13] E. A. M. van Alphen and W. J. M. de Jonge, Phys. Rev. B **51**, 8182 (1995).

[14] P. M. Petroff, A. C. Gossard, and W. Wiegmann, Appl. Phys. Lett. **45**, 620 (1984).

[15] P. Gambardella, M. Blanc, H. Brune, K. Kuhnke, and K. Kern, Phys. Rev. B **61**, 2254 (2000).

[16] P. Gambardella, M. Blanc, L. Bürgi, K. Kuhnke, and K. Kern, Surf. Sci. **449**, 93 (2000).

[17] V. E. Marsico, M. Blanc, K. Kuhnke, and K. Kern, Phys. Rev. Lett. **78**, 94 (1997).

[18] M. Blanc, K. Kuhnke, V. Marsico, and K. Kern, Surf. Sci. **414**, L964 (1998).

[19] *Helium Atom Scattering from Surfaces* edited by E. Hulpke, Springer Series in Surface Science Vol. 27 (Springer, Berlin, 1991).

[20] B. Poelsema, A. F. Becker, G. Rosenfeld, R. Kunkel, N. Nagel, L. K. Verheij, and G. Comsa, Surf. Sci. **272**, 269 (1992).

[21] F. Picaud, C. Ramseyer, C. Girardet, and P. Jensen, Phys. Rev. B **61**, 16 154 (2000).

[22] H. Röder, R. Schuster, H. Brune, and K. Kern, Phys. Rev. Lett. **71**, 2086 (1993).

[23] R. Q. Hwang, Phys. Rev. Lett. **76**, 4757 (1996).
[24] E. D. Tober, R. F. C. Farrow, R. F. Marks, G. Witte, K. Kalki, and D. D. Chambliss, Phys. Rev. Lett. **81**, 1897 (1998).
[25] K. Kuhnke, E. Hahn, R. David, P. Zeppenfeld, and K. Kern, Surf. Sci. **272**, 118 (1992).
[26] H. Schief, Ph.D. thesis, Ecole Polytechnique Fédérale de Lausanne, 1995.
[27] E. Hahn, H. Schief, V. Marsico, A. Fricke, and K. Kern, Phys. Rev. Lett. **72**, 3378 (1994).
[28] G. Comsa, G. Mechtersheimer, B. Poelsema, and S. Tomoda, Surf. Sci. **89**, 123 (1979).
[29] J. Lapujoulade, Y. Lejay, and N. Papanicolau, Surf. Sci. **90**, 133 (1979).
[30] B. Poelsema and G. Comsa, *Scattering of Thermal Energy Atoms from Disordered Surfaces*, Springer Tracts in Modern Physics Vol. 115 (Springer, Berlin, 1989).
[31] J. Tersoff, Physica E (Amsterdam) **3**, 89 (1998).
[32] J. Tersoff, Phys. Rev. Lett. **74**, 434 (1995).
[33] E. Bauer and J. H. van der Merwe, Phys. Rev. B **33**, 3657 (1986).
[34] H. L. Skriver and N. M. Rosengaard, Phys. Rev. B **46**, 7157 (1992).
[35] A. Christensen, A. V. Ruban, P. Stoltze, K. W. Jacobsen, H. L. Skriver, J. K. Nørskov, and F. Besenbacher, Phys. Rev. B **56**, 5822 (1997).
[36] J. Friedel, in *The Physics of Metals*, edited by J. M. Ziman (Cambridge University Press, Cambridge, 1969).
[37] M. C. Desjonqueres and D. Spanjaard *Concepts in Surface Physics* (Springer, Berlin, 1996).
[38] K. W. Jacobsen, J. K. Nørskov, and M. J. Puska, Phys. Rev. B **35**, 7423 (1987).
[39] M. S. Daw and M. I. Baskes, Phys. Rev. B **29**, 6443 (1984).
[40] F. Ercolessi, M. Parrinello, and E. Tosatti, Philos. Mag. A **58**, 213 (1988).
[41] M. W. Finnis and J. E. Sinclair, Philos. Mag. A **50**, 45 (1984).
[42] V. Rosato, M. Guiloppe, and B. Legrand, Philos. Mag. A **59**, 321 (1989).
[43] F. Ducastelle, Ph.D. thesis, Univ. Paris–Sud (1972).
[44] R. P. Gupta and H. L. Kharoo, J. Chem. Phys. **74**, 3577 (1981).
[45] M. C. Desjonquéres and D. Spanjaard, J. Phys. C **15**, 4007 (1982).
[46] G. Allan and M. Lannoo, Surf. Sci. **40**, 375 (1973).
[47] A. P. Sutton and J. Chen, Philos. Mag. Lett. **61**, 139 (1990).
[48] B. Legrand, Philos. Mag. **49**, 171 (1984).
[49] C. Mottet, R. Ferrando, F. Hontinfinde, and A. C. Levi, Surf. Sci. **417**, 220 (1998).
[50] J. Guevara, A. M. Llois, and M. Weissmann, Phys. Rev. B **52**, 11 509 (1995).
[51] E. S. Fisher and J. Renken, Phys. Rev. **135**, A482 (1964); E. S. Fisher and D. Dever, Acta Metall. Mater. **18**, 265 (1970).
[52] L. Vitos, A. V. Ruban, H. L. Skriver, and J. Kollar, Surf. Sci. **411**, 186 (1998).
[53] S. Briquez, A. Marmier, and C. Girardet, Langmuir **12**, 3969 (1996).
[54] P. Smilauer, M. R. Wilby, and D. D. Vvedensky, Surf. Sci. **291**, L733 (1993).
[55] F. Ducastelle, *Order and Phase Stability in Alloys*, Cohesion and Structure Vol. 3, edited by F. R. de Boer and D. G. Pettifor (North Holland, Amsterdam, 1991).
[56] H. Brune, Surf. Sci. Rep. **31**, 121 (1998).